The Role of Naphthalene and Its Derivatives in the Formation of Secondary Organic Aerosols in the Yangtze River Delta Region, China

Fei Ye[1], Jingyi Li[1], Yaqin Gao[2], Hongli Wang[2], Jingyu An[2,3], Cheng Huang[2], Song Guo[4], Keding Lu[4], Kangjia Gong[1], Haowen Zhang[1], Momei Qin[1], Jianlin Hu[1]

[1] Jiangsu Key Laboratory of Atmospheric Environment Monitoring and Pollution Control, Collaborative Innovation Center of Atmospheric Environment and Equipment Technology, School of Environmental Science and Engineering, Nanjing University of Information Science & Technology, Nanjing, 210044, China

[2] State Environmental Protection Key Laboratory of the Formation and Prevention of Urban Air Pollution Complex, Shanghai Academy of Environmental Sciences, Shanghai 200233, China

[3] Shanghai Key Laboratory of Atmospheric Particle Pollution and Prevention, Department of Environmental Science and Engineering, Fudan University, Shanghai 200438, China

[4] State Key Joint Laboratory of Environmental Simulation and Pollution Control, College of Environmental Sciences and Engineering, Peking University, Beijing, 100871, China

Correspondence: Jingyi Li (jingyili@nuist.edu.cn), Jianlin Hu (jianlinhu@nuist.edu.cn)

Abstract. Naphthalene (Nap) and its derivatives, including 1-methylnaphthalene (1-MN) and 2-methylnaphthalene (2-MN), serve as prominent intermediate volatile organic compounds (IVOCs) contributing to the formation of secondary organic aerosol (SOA). In this study, the Community Multiscale Air Quality (CMAQ) model coupled with detailed emissions and reactions of these compounds was utilized to examine their roles in the formation of SOA and other secondary pollutants in the Yangtze River Delta (YRD) region during summer. Significant underestimations of Nap and MN concentrations (by 79% and 85%) were observed at the Taizhou site based on the model results using the default emissions. Constrained by the observations, anthropogenic emissions of Nap and MN in the entire region were multiplied by 5 and 7, respectively, to better capture the evolution of pollutants. The average concentration of Nap reached 25 ppt in the YRD, with Nap contributing 4.1% and 8.1% (up to 12.6%) of total aromatic emissions and aromatic-derived secondary organic carbon (SOC), respectively. The concentrations of 1-MN and 2-MN were relatively low, averaging at 2 ppt and 5 ppt. Together, they accounted for only 2.4% of the aromatic-derived SOC. The impacts of Nap and MN oxidation on ozone and radicals were insignificant at regional scales but were not negligible when considering daily fluctuations in locations with high emissions of Nap and MN. This study highlights the significant roles of Nap and MN in the formation of SOA, which may pose environmental risks and adverse health effects.

1 Introduction

Secondary organic aerosols (SOA) are formed from the condensation and multiphase evolution of less volatile organic compounds (VOCs), which can be directly emitted or produced from the oxidation of higher volatile organics in the atmosphere. SOA not only affects visibility and human health but also exerts direct effects on the climate by absorbing and reflecting solar radiation, as well as indirect effects by influencing cloud formation (Chen et al., 2016; Zhang and

Ying, 2012). Semi-volatile and intermediate-volatile organic compounds (S/IVOCs) have been identified as the key precursors of SOA (Robinson et al., 2007; Hu et al., 2022). IVOCs are categorized by small polycyclic aromatic hydrocarbons (PAHs), intermediate-length alkanes (e.g. n-hexadecane), and phenols(Pye and Seinfeld, 2010). PAHs are organic compounds containing multiple aromatic rings. In 2004, China exhibited the highest annual PAH emissions (114 Gg) globally, accounting for 22% of the total emissions worldwide (Zhang and Tao, 2009). Naphthalene (Nap) and methylnaphthalene (MN), such as 1-methylnaphthalene (1-MN) and 2-methylnaphthalene (2-MN), are the most abundant airborne PAHs (Chen et al., 2016; Fang et al., 2021), primarily emitted from combustion of fossil fuels, biomass burning, and industrial sectors (Fang et al., 2021).

Chamber studies have identified the gas- and particle-phase products from Nap reacting with hydroxyl radicals (OH·) (Huang et al., 2019). Ring-retaining products (such as 1,4-naphthoquinone) with lower volatilities dominate under conditions of low nitrogen oxides (NO_x), and ring-opening products (such as 2-formyl cinnamaldehyde) with higher volatilities dominate in the presence of high NO_x. Chan et al. (2009) evaluated the SOA yields of Nap, 1-MN, 2-MN, and 1,2-dimethyl naphthalene in chambers to estimate SOA formation from primary emissions of diesel engines and wood burning. It was found that SOA is more efficiently produced under low-NO_x conditions than high-NO_x conditions, with yields of 55–75% and 25–45%, respectively, at a total organic aerosol loading of 15 μg m^{-3}. During photo-oxidation of less than 12 h, these PAHs produced 3–5 times more SOA than light aromatic compounds, accounting for up to 54% of the total SOA from the oxidation of diesel emissions. Huang et al. (2019) applied a tracer method to determine that 14.9% of SOA was attributed to the oxidation of Nap and MN in the afternoon during wintertime haze in Beijing. Shakya and Griffin (2010) also reported 37–162 kg day^{-1} of

SOA production from the mobile source emitted PAHs (including Nap, 1-MN, and 2-MN) in Houston, based on the yields from their study and that of Chan et al. (2009). By adopting the SOA yields from Shakya and Griffin (2010), Liu et al. (2015) showed that Nap accounted for 8–52% of the total SOA derived from benzene, toluene, C2-benzene, C3-benzene, C4-benzene, and Nap in exhaust emissions from light-duty gasoline vehicles. All these experimental findings demonstrate the significant role of Nap and MN in SOA formation in environments dominated by anthropogenic influences. However, these results might not accurately reflect the actual atmospheric conditions due to the simplicity of reaction conditions and the limited precursors involved in chamber studies (Ling et al., 2022).

Numerical models have been developed and utilized to assess the contribution of S/IVOCs to SOA (Hayes et al., 2015; Pye and Seinfeld, 2010; An et al., 2023). Zhang and Ying (2011) showed that PAHs emitted from anthropogenic sources could produce SOA mass as much as 10% of that from the traditional light aromatics or approximately 4% of the total anthropogenic SOA by using the Community Multiscale Air Quality (CMAQ) model. However, the SOA products of several PAH species such as Nap and MN were lumped together due to limited experimental data for explicit parameterization. Pye and Pouliot (2012) assumed that 10% of ARO2 (lumped aromatic species) reacted with OH· to represent SOA formation from PAHs in the CMAQ model, using Nap as a surrogate for parameterization, without considering individual PAH's emissions and OH· reactivity. According to Cohan et al. (2013), the modeled SOA increased by roughly 1–10% when Nap emissions from on-road gasoline and diesel vehicles were considered. Their simulations showed a lower limit in the SOA production from Nap due to underestimations in the emission inventory in the South Coast Air Basin of California. Majdi et al. (2019) found that Nap and MN contributed 2.4% of the total organic aerosol (OA) originating from wildfires over the Euro-

Mediterranean region during the summer of 2007 by using a 3D chemical transport model (CTM). The contributions of Nap and MN to SOA at regional scales in China had not been quantified.

In this study, SOA formation from Nap, 1-MN, and 2-MN in the Yangtze River Delta (YRD) region during the EXPLORE-YRD (EXPeriment on the eLucidation of the atmospheric Oxidation capacity and aerosol foRmation and their Effects in the Yangtze River Delta) campaign period (May 20 − June 18, 2018) was investigated by using an updated CMAQ model that incorporated explicit SOA schemes for these PAHs. Emission inventories of Nap, 1-MN, and 2-MN were estimated based on different sources and methods and validated against observations. After that, the influences of Nap and MN on secondary organic carbon (SOC), ozone (O_3), and radical concentrations were examined in locations with high levels of Nap and MN as well as at the regional scale. The newly added SOA parameterizations for 1-MN and 2-MN were fitted by both two-product and one-product methods to compare the differences. We found that Nap and its derivatives, although accounting for a small fraction of emitted aromatics (5.1%), contributed 10.4% of aromatic-derived SOC in the YRD.

2 Methods

2.1 Modified SOA formation pathways of MN

The CMAQ model version 5.2, coupled with the SAPRC07tic atmospheric chemical mechanism and the AERO6i aerosol module, was updated to include the oxidation of 1-MN and 2-MN by OH· and the corresponding SOA formation pathways. In the original CMAQ model, Nap reacts with OH· to form SOA under high- and low-NO_x conditions, represented by two different counter species PAHNRXN and PAHHRXN, respectively (Fig. 1a). Similar to Nap, 1-MN, and 2-MN were explicitly treated as reacting with OH· and forming SOA counter species under high NO_x (aMPAHNRXN and bMPAHNRXN) and low NO_x (aMPAHHRXN and bMPAHHRXN),

along with other products following Zhang and Ying (2012). These counter species were used to calculate the production of SOA through gas-particle partitioning based on yields (α_i) and partitioning coefficients ($K_{\mathrm{om},i}$, $\mathrm{m^3\ \mu g^{-1}}$) of condensable organic products derived from chamber experiment data. Details of gas-particle partitioning for fitting SOA formation using one-product and two-product methods are described in the Supplement.

In the original CMAQ model, a two-product method (SV_PAH1 and SV_PAH2) was used to represent the SOA formation from Nap under high-NO_x conditions, denoted as APAH1J and APAH2J, respectively (Fig. 1a). Under low-NO_x conditions, a one-product method was used to represent the SOA formation from Nap, denoted as APAH3J. It was assumed that APAH3J (with a yield of α_3) was non-volatile and resided in the particle phase. Similar to Nap, a two-product method for the SOA formation from 1-MN under high-NO_x conditions was added as shown in Fig. 1b, with the SOA species denoted as AaMPAH1J and AaMPAH2J. Additionally, a one-product method characterizing the SOA formation from 1-MN under high-NO_x conditions was applied to compare differences caused by different fitting approaches. As shown in Fig. 1c, the semi-volatile organic product SV_aMPAH1' undergoes equilibrium partitioning to form SOA (AaMPAH1J'). Under low-NO_x conditions, a non-volatile SOA product AaMPAH3J is formed through oxidation of 1-MN. The SOA scheme of 2-MN followed that of 1-MN with corresponding products AbMPAH1J and AbMPAH2J (or AbMPAH1J') under high-NO_x conditions and AbMPAH3J under low-NO_x conditions, respectively. Moreover, all semi-volatile SOA products originating from MN undergo condensed-phase oligomerization reactions at the same rate as APAH1J and APAH2J, generating anthropogenic non-volatile oligomers (AOLGAJ). Other processes and parameters involved in the newly added SOA pathways for 1-MN and 2-MN, such as the dry and wet deposition and the molecular weight of the oxidation products, were set to be the same as Nap

due to limited experimental data. Details of all the parameters, i.e., α_i, $K_{\mathrm{om},i}$, and $\Delta H_{\mathrm{vap},i}$ are summarized in Table S1.

2.2 Model application

The simulation domain, which covers Jiangsu, Zhejiang, Anhui, Shanghai, and neighboring provinces, has a horizontal resolution of 4 km × 4 km (238 × 268 grids) and a vertical structure of 18 layers as shown in Fig. S1. Details of the domain setup can be found in previous studies (Li et al., 2022; Li et al., 2021). The meteorological field was predicted by the Weather Research and Forecasting (WRF) model version 4.0 with the ECMWF Reanalysis v5.0 (ERA5) reanalysis data as inputs. More details about the WRF configuration have been summarized by Wang et al. (2021). A spin-up of two days was used to minimize the influence of initial conditions.

Biogenic emissions were generated from the Model for Emissions of Gases and Aerosols from Nature (MEGAN) version 2.1 (Guenther et al., 2012). Open biomass burning emissions were based on the Fire INventory from the National Center for Atmospheric Research (FINN) (Wiedinmyer et al., 2011). Anthropogenic emissions were generated from the updated 2017 emission inventory for the YRD (Cheng et al., 2021) and the Multi-resolution Emission Inventory for China (MEIC, http://www.meicmodel.org, last access: 1 June 2023) for the rest of the domain. Currently, there is a lack of localized source profiles in China, particularly regarding Nap and MN. These data were obtained from the U.S. Environmental Protection Agency's (EPA's) repository of organic gas and particulate matter (PM) speciation profiles of air pollution sources (SPECIATEv5.2) along with the source information reported by An et al. (2021) and Li et al. (2014). Relevant details of emission calculations can be found in the Supplement. There are two sets of emission data consisting of different Nap and MN emissions. The emis-orig used the original Nap emissions from the 2017 YRD inventory as well as the calculated Nap emissions in

the rest of the domain and MN emissions in the entire domain. We show later that Nap and MN were underestimated and required an adjustment in their emissions to capture the observed concentrations. Considering their predominantly anthropogenic origin, their anthropogenic emissions in the entire region from emis-orig were multiplied by 5 and 7 respectively in the emis-adjust case. All the emission ratios applied in this study are shown in Table S2. According to Fig. S2, Nap and MN emissions were mainly located in Shanghai, southern Jiangsu, and parts of Zhejiang. After adjustments, the total emission rate of Nap and MN in the YRD region in emis-adjust (85.0 tons day^{-1}) was approximately 4 times higher than that in emis-orig (18.2 tons day^{-1}). The total MN emission rate in the YRD region in emis-adjust was 20.3 tons day^{-1}, lower than that of Nap. For emis-adjust, the dominant source of MN was residential-related (47.0%), followed by industry process (25.8%) and on-road transportation (20.8%). Among all sources, on-road transportation contributed the most to Nap emissions in both emis-orig (78.2%) and emis-adjust (87.5%). It should be noted that uncertainties associated with the emission inventory and source profiles, which are based on sector-specific mass ratios presented in Table S2, may potentially affect both the distribution and source contributions of Nap and MN.

Table 1 lists the scenarios conducted in this study. In case-1product-orig, the anthropogenic emissions were based on emis-orig, along with the SOA parameterization for MN fitted by a one-product method in Fig. 1c and that of Nap fitted by a two-product method in Fig. 1a under high-NO_x conditions. To assess the impacts of different SOA parameterizations, case-2products-orig adopted the same setting as case-1product-orig except for utilizing a two-product method for MN-derived SOA under high-NO_x conditions (Fig. 1b). For accurate representations of the fate of Nap and MN in the atmosphere, both case-1product and case-2products employed adjusted emissions (emis-adjust) along with different SOA parameterizations for MN. SOA formation from Nap and

MN under low-NO_x conditions in the above cases were all characterized by a fixed yield as shown in Table S1. Overall, the contributions of Nap, 1-MN, and 2-MN to the aromatic SOC were estimated based on different emission inventories and SOA schemes. To evaluate the effects of Nap, 1-MN, and 2-MN on O_3, SOC, and radical concentrations, their emissions in case-1product were set to zero and named base_zeroNapMN. A case named base_zeroMN was conducted to quantify the individual effects of Nap and MN by setting the emissions of 1-MN and 2-MN to zero.

2.3 Observation data for model validation

In May-June 2018, the EXPLORE-YRD field campaign was launched at a rural site in Taizhou (32.558°N, 119.994°E) and simultaneously monitored VOCs (including Nap and MN), O_3, NO_x, organic carbon (OC), OH·, hydroperoxy radical (HO_2·), and other various pollutants, which provides a good opportunity for model validation and understanding the evolution of air pollution in the YRD (Wang et al., 2020a; Huang et al., 2020; Yu et al., 2021; Gao et al., 2022). Details of the measurement method and accuracy for each species refer to these references. The simulated daily maximum 8-hour average (MDA8) O_3, fine particulate matter ($PM_{2.5}$), sulfur dioxide (SO_2), nitrogen dioxide (NO_2), and carbon monoxide (CO) were also compared with the observations from the National Real-Time Urban Air Quality Release Platform of the China Environmental Monitoring Center (http://106.37.208.233:20035/, last access on May 17, 2023) in Suzhou, Nanjing, Hangzhou, Hefei, and Shanghai cities as shown in Fig. S1. The statistical metrics including normalized mean bias (NMB), normalized mean error (NME), and correlation coefficient (r) were calculated for several air pollution species. The benchmarks for model performance followed the recommendations by Emery et al. (2017) and are listed in Table S3. The meteorological parameters predicted by WRF have been examined to be robust during the same episode by Wang et al. (2021).

3 Results

3.1 Model validation

Figure 2 and Fig. S3 show the comparison of observed and simulated hourly variations of Nap, MN, O_3, OC, and $PM_{2.5}$ at the Taizhou site during the study period. The concentrations of Nap in case-1product-orig and case-2products-orig were significantly underestimated by 79% compared to the observations. In contrast, emis-adjust better represented the temporal variations of Nap (NMB=0.01, r=0.68) than emis-orig, with the average concentration increasing by a factor of 4 and agreeing well with the observations. The modeled concentration of MN by emis-adjust (14.0 ppt) was also comparable to the observed value (15.0 ppt) and showed a good correlation between the two (r=0.59). For other species, the concentrations of OC and $PM_{2.5}$ were slightly increased in emis-adjust compared to that of emis-orig, although they were underestimated in both scenarios. The NMB and NME of $PM_{2.5}$ satisfied the benchmarks recommended by Emery et al. (2017), while the NMB of MDA8 O_3 exceeded the criteria. Table S4 shows that the concentrations of NO_2 and nitric oxide (NO) were underestimated at the Taizhou site. The simulated OH radicals agreed well with observations while the concentrations of HO_2· were underestimated at the Taizhou site (Fig. S4). It should be noted that the influences of different SOA schemes for MN on the aforementioned species are negligible. The predicted concentrations of MDA8 O_3, $PM_{2.5}$, SO_2, NO_2, and CO in other cities were also examined. Overall, the model agreed well with observations except for a significant underestimation of MAD8 O_3 in Shanghai (Table S3). The results of case-1product and case-2products using emis-adjust as the emission data were superior compared to the cases using emis-orig. These findings will be further discussed in the subsequent analysis.

3.2 Influences of Nap and MN on SOC in Taizhou

Figure 3 depicts the diurnal variations of emissions and concentrations of Nap, 1-MN, and 2-MN, as well as the corresponding SOC products SOC-Nap, SOC-1MN, and SOC-2MN at the Taizhou site in both case-1product and case-2products. The emissions of Nap, 1-MN, and 2-MN exhibited a bimodal pattern. For Nap, the bimodal characteristics were the most pronounced, accompanied by two peaks that occurred between 8:00~9:00 and 16:00~17:00, respectively. This is likely attributed to the dominant source of Nap from transportation as described in Sect. 2.2. Nap and MN concentrations were relatively low during the daytime and peaked in the morning and at night. This is caused by the fast photochemical removal and increased dilution during the daytime, along with the facilitated accumulation due to low mixing heights at night (Huang et al., 2019; Cohan et al., 2013). The simulated diurnal variation of Nap agreed well with observations, but the daytime MN concentration was underpredicted as shown in Fig. S5. The concentrations of SOC generated by Nap, 1-MN, and 2-MN were high during the daytime, especially from 10:00 to 15:00. This is attributed to the removal of Nap and MN by OH radicals to form SOC. The potential removal by nitrate radicals (NO_3) was negligible in this study, leading to a decline in SOC formation at night. Nap-derived SOC was the most abundant, followed by SOC from 2-MN and 1-MN. This is attributed to the combined effects of the OH· reactivity, SOA yields, as well as abundances of the three compounds (Li et al., 2017; Yu et al., 2021). Apart from having the highest emissions, Nap also exhibits greater reactivity with OH·. Although its SOA yield under high-NO_x conditions is lower than that of MN fitted by the one-product scheme (Fig. S6), its SOA yield under low-NO_x conditions is the highest among the three PAHs (Table S1). Overall, Nap contributed the most to SOC. 2-MN demonstrates higher SOA yields than 1-MN under high-NO_x conditions in both cases, but a lower SOA yield under low-NO_x conditions. Considering the impact of a higher emission rate (Fig. 3a and 3c), 2-MN contributed two times more SOC compared to 1-

MN. The SOC generated by MN in case-2products was lower than that in case-1product due to the lower SOA yield applied in case-2products (Fig. S6).

Figure 4 shows the contributions of major aromatic species, i.e., Nap, 1-MN, 2-MN, 1,2,4-trimethyl benzene (B124), xylene (MPO), benzene (BENZ), toluene (TOLU), aromatics with k_{OH} (reaction rate constant with OH·) < 2×10^4 ppm^{-1} min^{-1} (ARO1) and ARO2MN' (ARO2 excluding Nap and MN) to the total emissions of aromatics and the aromatic-derived SOC in both case-1product and case-2products at the Taizhou site. Among all the species, ARO2MN', MPO, and B124 showed the largest fraction in emissions, accounting for 58.6%, followed by ARO1 and TOLU (31.8%), and BENZ (6.3%). Nap and MN contributed the least to the total aromatic emissions, with Nap being the most abundant species. The daily average concentrations of SOC produced from all the aromatics were quite similar in case-1product and case-2products, with the values of 101.3 and 100.2 ng m^{-3}, respectively (Fig. S7). The contribution of ARO2MN', MPO, and B124 to the total aromatic-derived SOC was the most significant, ranging from 45.6% to 46.2%. Nap indicated a remarkable contribution to SOC, accounting for 8.2–8.3%, despite constituting only 2.6% of the total emitted aromatics. 2-MN was also an important SOC precursor, contributing 1.2–2.0% of the aromatic-derived SOC. 1-MN showed the lowest emissions, accounting for 0.2% of the total aromatic emissions and less than 1.0% of the aromatic-derived SOC. Overall, Nap, 1-MN, and 2-MN exhibited the same trait of contributing significantly more to SOC than to precursor emissions, especially for Nap. The total contributions of MN and Nap to SOC were higher than that of BENZ, even though their emissions were significantly lower than BENZ. Similar results were also found in field campaigns conducted in Guangzhou (Fang et al., 2021) and Beijing (Huang et al., 2019) where Nap and MN showed higher contributions. Compared to benzene and other monocyclic aromatics, the oxidation products of Nap and MN are

much less volatile and are more efficient at aerosol growth (Wang et al., 2020b). Thus, their considerably higher SOA yields and reactivity with OH· lead to an important contribution to SOA formation. We found that 3.3% of aromatic emissions from Nap and derivatives contributed up to 10.9% of SOC generated from aromatics at the Taizhou site.

3.3 Regional distributions of Nap and MN and the influences on secondary pollutants

In the YRD, Nap accounted for 4.1% of aromatic emissions and contributed 8.0% and 8.1% of the total SOC generated by aromatics in case-1product and case-2products, respectively (Fig. S8). We found extremely high contributions of Nap-derived SOC in areas with high Nap emissions, reaching up to 12.6% in case-2products. 2-MN contributed 0.6% of the total aromatic emissions and up to 2.5% of the aromatic-derived SOC in case-1product. Among the three PAHs, 1-MN showed the lowest emissions (about 0.4% of the aromatic emissions) and contributed minimally to the regional average SOC (0.4–0.7%). The SOC derived from MN in case-2products was approximately 38% lower than that in case-1product across the entire YRD region (Fig. S9), while minor differences were observed in O_3 and the total SOC between the two cases with different SOA parameterization of MN (Fig. S10). In general, the concentrations of SOC produced by the three PAHs in case-1product were higher than that in case-2products, exhibiting similar spatial distribution patterns in both cases. We will focus on the results from case-1product in the subsequent analysis.

Accurate representation of Nap and MN sources and sinks in model simulations is crucial for comprehending the atmospheric oxidation capacity. The relative differences between base_zeroNapMN and case-1product were calculated to evaluate the effects of Nap, 1-MN, and 2-MN on O_3, SOC, and radical concentrations. As shown in Fig. 5a, the SOC concentrations in the YRD increased by approximately 0.9% on average, with the most significant change observed in

areas with high emissions of Nap and MN, such as Shanghai and southern Jiangsu Province, reaching up to 1.7%. The impact on O_3 was relatively limited, with a maximum increase of 0.3%, primarily attributed to Nap rather than MN (Fig. S11). Similar to SOC, the spatial distribution of O_3 variations was consistent with that of Nap and MN emissions. By considering the oxidation of Nap and MN in the model, HO_2· concentration was enhanced across the domain by up to 1.6% (in Shanghai), likely due to the production of HO_2· through the reaction of Nap and MN with OH·. However, the variations in OH· concentration exhibited regional heterogeneity, with a maximum increase of 0.7% in Shanghai and a maximum decrease of 0.3% in Wenzhou. The areas with elevated OH· coincided with the locations experiencing notable increases in O_3. As an OH· source in the troposphere, the photolysis of O_3 produces electronically excited $O(^1D)$ atoms that react with water molecules to form fresh OH· (Qin et al., 2022; Tan et al., 2019). Moreover, the areas with elevated OH· also exhibited a significant increase in HO_2·. HO_2· can react with O_3 or NO to produce OH·, thereby offsetting the OH· consumption by Nap and MN oxidation (Zhu et al., 2020). In the areas with decreased OH·, the increases of O_3 and HO_2· were insignificant, resulting in a reduced generation of OH· to compensate for the OH· consumption by Nap and MN. Similar to O_3, variations in OH· and HO_2· were primarily influenced by Nap rather than MN (Fig. S11).

To avoid obscuring the true magnitude by averaging over the entire episode, daily relative differences of SOC, O_3, and radicals at the Shanghai and Suzhou sites, which exhibit significant variations, are shown in Fig. 5b and 5c. Overall, the influences of Nap and MN varied daily. At the Shanghai site, the most pronounced effects on OH· and HO_2· were observed, with increases of up to 1.9% and 3.8%, respectively. At the Suzhou site, the maximum daily variations of OH· and HO_2· (1.5% and 2.9%) were slightly lower than those in Shanghai. However, the daily SOC and O_3 were elevated by up to 3.0% and 1.1% in Suzhou, respectively. It was found that both OH· and

316 HO_2· displayed bimodal variations at the two sites, with the most pronounced changes of 0.7–1.0%
317 and 1.6–2.2% occurring in the morning, respectively (Fig. S12). The concentrations of SOC and
318 O_3 were elevated in the daytime, reaching peak increments of 2.1–2.3% and 0.4–0.5% at noon.
319 Consequently, the influences of Nap and MN on SOC, O_3, and the atmospheric oxidation capacity
320 were substantial at the daily scale in those regions.

321 **4 Discussion**

322 Our results revealed that the contributions of Nap and MN to the total aromatic emissions
323 were minimal, which were 5.1% in the YRD and 3.3% at the Taizhou site. However, the SOC
324 produced by Nap and MN accounted for 10.4% of the total aromatic-derived SOC in this region
325 and 10.9% at the Taizhou site. Given the overestimation of other aromatic species in the current
326 model (Table S4), the contributions of Nap and MN to aromatic SOC may be underestimated. Yu
327 et al. (2021) demonstrated an augmented fraction of SOC derived from a yield method to that using
328 the EC tracer method after the inclusion of Nap and MN oxidation (from 25.3% to 39.5%) during
329 the same episode at the Taizhou site. That is to say, Nap and MN contribute 35.9% of the total
330 SOC estimated by using the SOA yield multiplied by the consumption of VOCs, which is higher
331 than the value (10.9%) in this study. Other field studies have also found significant SOA formation
332 from Nap and MN among aromatics in the Pearl River Delta region (12.4%) (Fang et al., 2021)
333 and in Beijing during haze days (10.2±1.3%) (Huang et al., 2019), with relatively smaller
334 contributions to emissions of aromatics by less than 2% and 7%, respectively. This study highlights
335 the important roles of Nap and MN, which exhibit high SOA formation potentials with trace
336 amounts emitted into the atmosphere. In addition, the average concentrations of Nap and MN in
337 this study were 25 and 7 ppt during summer over the YRD region (Fig. S9), respectively. Previous
338 studies have confirmed that the concentrations of Nap and MN exhibited a seasonal variation, with

maxima in winter and minima in summer, attributed to the increased heating and cooking activities in households during the cold season (Huang et al., 2019; Fang et al., 2021; Tang et al., 2020). Consequently, the ambient concentration of Nap and MN, along with the potential SOA production may be more severe in winter. Cleaner fuel types and household cleaning products are recommended for vehicular and domestic usage.

The improvement in simulation and assessment of Nap and MN chemistry is crucial. Firstly, the characterization of Nap and MN from local sources and additional field observations are indispensable to reduce the disparities between the modeled and observed Nap and MN concentrations. Secondly, the SOA parameterizations of Nap and MN, including the enthalpy of vaporization and SOA yields, are derived from limited chamber experiments and require further validation. Previous studies have reported that the SOA yields obtained from chamber studies were contingent on OH· exposure, NO_x levels, relative humidity, and seed particles, which may not represent the actual atmospheric conditions (Yu et al., 2021; Ling et al., 2022). Thirdly, chlorine radicals (Cl), NO_3 radicals, and O_3 also play an important role in the atmospheric reactions of Nap and MN (Wang et al., 2005; Cohan et al., 2013; Riva et al., 2015, 2014; Aleman, 2006), which were missing in the current study due to the lack of parameterization. The formation of gas- and particle-phase products through reactions between Cl atoms and Nap has been confirmed. For instance, chloronaphthalene and chloroacenaphthenone have been identified as potential SOA markers for the Cl-initiated oxidation of Nap in the ambient atmosphere (Riva et al., 2015). As important sources of Cl atoms, abundant nitryl chloride ($ClNO_2$) and molecular chlorine (Cl_2) are attributed to sea salt, coal combustion, biomass burning (Le Breton et al., 2018), and urban-originated transport (Li et al., 2021; Tham et al., 2014). Consequently, the Cl-initiated SOA formation process may be pronounced in specific regions, such as the marine boundary layer and

industrial areas. Using the rate constant of Cl with Nap ($(4.22\pm0.46)\times10^{-12}$) (Riva et al., 2014) and corresponding SOA yields (0.91±0.05) (Riva et al., 2015), which is up to three times higher than those determined from OH-initiated oxidation (Chan et al., 2009; Shakya and Griffin, 2010), we estimated the potential SOA formation from the reaction of Nap and Cl atoms via a yield method (Huang et al., 2019; Yu et al., 2021). Assuming a 12-h average daytime OH· concentration of 2×10^{6} molecules cm^{-3} and a photooxidation age of 6 h, the SOA generated from Nap oxidation by Cl atoms can reach up to 56% of that from the Nap + OH pathway in highly polluted regions with a Cl/ OH ratio greater than 0.8 (Choi et al., 2020). This suggests that the omission of Cl-initiated chemistry in this study might lead to an underestimation of Nap-derived SOA by approximately 36%. Given the underestimation of anthropogenic chlorine emissions in China (Choi et al., 2020; Li et al., 2021), further studies are recommended to estimate chlorine emissions with finer spatial resolution and the impacts on Nap SOA under atmospherically realistic conditions. Lastly, a precise depiction of Nap and MN chemistry is crucial for gaining a deeper understanding of the health implications of these noxious compounds. The health risks associated with inhalation exposure to outdoor Nap and other PAHs have been assessed by calculating the incremental lifetime cancer risk (ILCR) values in China and the United States (Han et al., 2020; Zhang et al., 2016). Nonetheless, there has been no systematic evaluation of the health risks resulting from exposure to PAH-derived SOA and by-products, despite previous studies verifying the toxicological impacts (e.g. oxidation potential, OP) of Nap-derived SOA (Wang et al., 2018; Tuet et al., 2017a; Tuet et al., 2017b; Lima de Albuquerque et al., 2021). More precise measurements of the OP of different SOA components are needed to evaluate the overall oxidative potentials of ambient SOA. Future studies are needed to develop rational parameterization schemes for assessing the health risks associated with Nap- and MN-derived SOA.

5 Conclusions

In this study, we investigated the impacts of Nap, 1-MN, and 2-MN oxidation on the formation of SOC, O_3, and radicals from May 20 to June 18, 2018, in the YRD using a revised CMAQ model and explicit emission inventories. The results of case-1product, using the adjusted emissions (emis-adjust) and a one-product method for fitting MN SOA, best captured the observed evolution of Nap (NMB=0.01) and MN (NMB=-0.07) when compared to the default case (NMB=-0.79 for Nap, NMB=-0.85 for MN). The primary sources of Nap and MN were transportation and residential-related sectors, resulting in a bimodal emission pattern. The concentrations of Nap and MN were lowest during the daytime, peaking in the morning and at night. Their SOC concentrations reached the maximum value during the daytime due to the photooxidation of Nap and MN and boundary layer evolution. Nap, 1-MN, and 2-MN exhibited the same trait of contributing more to aromatic-derived SOC than to emissions of aromatic hydrocarbons, especially for Nap. The average concentration of Nap was 25 ppt in the YRD, accounting for 4.1% and 8.1% (up to 12.6%) of total aromatic emissions and aromatic-derived SOC, respectively. The concentrations of 1-MN and 2-MN were relatively low, with average values of 2 ppt and 5 ppt, respectively, Together, they contributed only 2.4% of the aromatic-derived SOC. At the regional scale, the impacts of Nap and MN oxidation on O_3 and radical concentrations were limited. However, substantial increases still occurred in areas with high Nap and MN emissions, which cannot be ignored. The high SOA formation potentials of Nap and MN and their impacts on secondary pollutants highlight the importance of considering these IVOCs alongside traditional VOCs when implementing air pollution control policies, energy use strategies, and health risks evaluation.

Code and data availability

The codes used for all the analyses are available on reasonable request to the corresponding author. All data used in this research are freely available and may be downloaded from the links and cited references given in the methods section.

Author contributions

F.Y., J.L., and J.H. designed the research and conducted the simulations. Y.G., H.W., S.G., and K.L. collected the observation data. J.A. and C.H. provided emission data. F.Y. led data analysis and drafted the main text. J.L., J.H., and M.Q. analyzed the data. All authors contributed to interpreting the results and editing the manuscript.

Competing interests

The authors declare no competing interests.

Disclaimer

Publisher's note: Copernicus Publications remains neutral with regard to jurisdictional claims made in the text, published maps, institutional affiliations, or any other geographical representation in this paper. While Copernicus Publications makes every effort to include appropriate place names, the final responsibility lies with the authors.

Acknowledgements

This work was financially supported by the National Key R&D Program of China (2022YFE0136200) and the National Natural Science Foundation of China (No. 42077199).

References

Aleman, G.: The kinetics and mechanisms of chlorine atom reactions with alkylbenzenes and alkylnaphthalenes, M.S., California State University, Fullerton., 148 pp., 2006.

An, J., Huang, C., Huang, D., Qin, M., Liu, H., Yan, R., Qiao, L., Zhou, M., Li, Y., Zhu, S., Wang, Q., and Wang, H.: Sources of organic aerosols in eastern China: a modeling study with high-

resolution intermediate-volatility and semivolatile organic compound emissions, Atmos. Chem. Phys., 23, 323-344, 10.5194/acp-23-323-2023, 2023.
An, J., Huang, Y., Huang, C., Wang, X., Yan, R., Wang, Q., Wang, H., Jing, S. a., Zhang, Y., Liu, Y., Chen, Y., Xu, C., Qiao, L., Zhou, M., Zhu, S., Hu, Q., Lu, J., and Chen, C.: Emission inventory of air pollutants and chemical speciation for specific anthropogenic sources based on local measurements in the Yangtze River Delta region, China, Atmos. Chem. Phys., 21, 2003-2025, 10.5194/acp-21-2003-2021, 2021.
Chan, A. W. H., Kautzman, K. E., Chhabra, P. S., Surratt, J. D., Chan, M. N., Crounse, J. D., Kürten, A., Wennberg, P. O., Flagan, R. C., and Seinfeld, J. H.: Secondary organic aerosol formation from photooxidation of naphthalene and alkylnaphthalenes: implications for oxidation of intermediate volatility organic compounds (IVOCs), Atmos. Chem. Phys., 9, 3049-3060, 10.5194/acp-9-3049-2009, 2009.
Chen, C.-L., Kacarab, M., Tang, P., and Cocker, D. R.: SOA formation from naphthalene, 1-methylnaphthalene, and 2-methylnaphthalene photooxidation, Atmos. Environ., 131, 424-433, 10.1016/j.atmosenv.2016.02.007, 2016.
Cheng, Y., Yu, Q.-q., Liu, J.-m., Du, Z.-Y., Liang, L.-l., Geng, G.-n., Zheng, B., Ma, W.-l., Qi, H., Zhang, Q., and He, K.-b.: Strong biomass burning contribution to ambient aerosol during heating season in a megacity in Northeast China: Effectiveness of agricultural fire bans?, Sci. Total Environ., 754, 142144, https://doi.org/10.1016/j.scitotenv.2020.142144, 2021.
Choi, M. S., Qiu, X., Zhang, J., Wang, S., Li, X., Sun, Y., Chen, J., and Ying, Q.: Study of Secondary Organic Aerosol Formation from Chlorine Radical-Initiated Oxidation of Volatile Organic Compounds in a Polluted Atmosphere Using a 3D Chemical Transport Model, Environ. Sci. Technol., 54, 13409-13418, 10.1021/acs.est.0c02958, 2020.
Cohan, A., Eiguren-Fernandez, A. J. I. J. o. E., and Pollution: Secondary organic aerosol formation from naphthalene roadway emissions in the South Coast Air Basin of California, Int. J. Environ. Pollut., 52, 206-224, 2013.
Emery, C., Liu, Z., Russell, A. G., Odman, M. T., Yarwood, G., and Kumar, N.: Recommendations on statistics and benchmarks to assess photochemical model performance, J. Air Waste Manage. Assoc., 67, 582-598, 10.1080/10962247.2016.1265027, 2017.
Fang, H., Luo, S., Huang, X., Fu, X., Xiao, S., Zeng, J., Wang, J., Zhang, Y., and Wang, X.: Ambient naphthalene and methylnaphthalenes observed at an urban site in the Pearl River Delta region: Sources and contributions to secondary organic aerosol, Atmos. Environ., 252, 10.1016/j.atmosenv.2021.118295, 2021.
Gao, Y., Wang, H., Liu, Y., Zhang, X., Jing, S., Peng, Y., Huang, D., Li, X., Chen, S., Lou, S., Li, Y., and Huang, C.: Unexpected High Contribution of Residential Biomass Burning to Non-Methane Organic Gases (NMOGs) in the Yangtze River Delta Region of China, J. Geophys. Res.-Atmos., 127, 10.1029/2021jd035050, 2022.
Guenther, A. B., Jiang, X., Heald, C. L., Sakulyanontvittaya, T., Duhl, T., Emmons, L. K., and Wang, X.: The Model of Emissions of Gases and Aerosols from Nature version 2.1 (MEGAN2.1): an extended and updated framework for modeling biogenic emissions, Geosci. Model Dev., 5, 1471-1492, 10.5194/gmd-5-1471-2012, 2012.
Han, F., Guo, H., Hu, J., Zhang, J., Ying, Q., and Zhang, H.: Sources and health risks of ambient polycyclic aromatic hydrocarbons in China, Sci Total Environ, 698, 134229, 10.1016/j.scitotenv.2019.134229, 2020.
Hayes, P. L., Carlton, A. G., Baker, K. R., Ahmadov, R., Washenfelder, R. A., Alvarez, S., Rappenglück, B., Gilman, J. B., Kuster, W. C., de Gouw, J. A., Zotter, P., Prévôt, A. S. H., Szidat,

S., Kleindienst, T. E., Offenberg, J. H., Ma, P. K., and Jimenez, J. L.: Modeling the formation and aging of secondary organic aerosols in Los Angeles during CalNex 2010, Atmos. Chem. Phys., 15, 5773-5801, 10.5194/acp-15-5773-2015, 2015.
Hu, W., Zhou, H., Chen, W., Ye, Y., Pan, T., Wang, Y., Song, W., Zhang, H., Deng, W., Zhu, M., Wang, C., Wu, C., Ye, C., Wang, Z., Yuan, B., Huang, S., Shao, M., Peng, Z., Day, D. A., Campuzano-Jost, P., Lambe, A. T., Worsnop, D. R., Jimenez, J. L., and Wang, X.: Oxidation Flow Reactor Results in a Chinese Megacity Emphasize the Important Contribution of S/IVOCs to Ambient SOA Formation, Environ. Sci. Technol., 56, 6880-6893, 10.1021/acs.est.1c03155, 2022.
Huang, D. D., Kong, L., Gao, J., Lou, S., Qiao, L., Zhou, M., Ma, Y., Zhu, S., Wang, H., Chen, S., Zeng, L., and Huang, C.: Insights into the formation and properties of secondary organic aerosol at a background site in Yangtze River Delta region of China: Aqueous-phase processing vs. photochemical oxidation, Atmos. Environ., 239, 117716, https://doi.org/10.1016/j.atmosenv.2020.117716, 2020.
Huang, G., Liu, Y., Shao, M., Li, Y., Chen, Q., Zheng, Y., Wu, Z., Liu, Y., Wu, Y., Hu, M., Li, X., Lu, S., Wang, C., Liu, J., Zheng, M., and Zhu, T.: Potentially Important Contribution of Gas-Phase Oxidation of Naphthalene and Methylnaphthalene to Secondary Organic Aerosol during Haze Events in Beijing, Environ. Sci. Technol., 53, 1235-1244, 10.1021/acs.est.8b04523, 2019.
Le Breton, M., Hallquist, Å. M., Pathak, R. K., Simpson, D., Wang, Y., Johansson, J., Zheng, J., Yang, Y., Shang, D., Wang, H., Liu, Q., Chan, C., Wang, T., Bannan, T. J., Priestley, M., Percival, C. J., Shallcross, D. E., Lu, K., Guo, S., Hu, M., and Hallquist, M.: Chlorine oxidation of VOCs at a semi-rural site in Beijing: significant chlorine liberation from ClNO2 and subsequent gas- and particle-phase Cl–VOC production, Atmos. Chem. Phys., 18, 13013-13030, 10.5194/acp-18-13013-2018, 2018.
Li, J., Zhang, M., Wu, F., Sun, Y., and Tang, G.: Assessment of the impacts of aromatic VOC emissions and yields of SOA on SOA concentrations with the air quality model RAMS-CMAQ, Atmos. Environ., 158, 105-115, 10.1016/j.atmosenv.2017.03.035, 2017.
Li, J., Zhang, N., Wang, P., Choi, M., Ying, Q., Guo, S., Lu, K., Qiu, X., Wang, S., Hu, M., Zhang, Y., and Hu, J.: Impacts of chlorine chemistry and anthropogenic emissions on secondary pollutants in the Yangtze river delta region, Environ. Pollut., 287, 117624, https://doi.org/10.1016/j.envpol.2021.117624, 2021.
Li, L., Xie, F., Li, J., Gong, K., Xie, X., Qin, Y., Qin, M., and Hu, J.: Diagnostic analysis of regional ozone pollution in Yangtze River Delta, China: A case study in summer 2020, Sci. Total Environ., 812, 151511, 10.1016/j.scitotenv.2021.151511, 2022.
Li, M., Zhang, Q., Streets, D. G., He, K. B., Cheng, Y. F., Emmons, L. K., Huo, H., Kang, S. C., Lu, Z., Shao, M., Su, H., Yu, X., and Zhang, Y.: Mapping Asian anthropogenic emissions of non-methane volatile organic compounds to multiple chemical mechanisms, Atmos. Chem. Phys., 14, 5617-5638, 10.5194/acp-14-5617-2014, 2014.
Lima de Albuquerque, Y., Berger, E., Tomaz, S., George, C., and Géloën, A.: Evaluation of the Toxicity on Lung Cells of By-Products Present in Naphthalene Secondary Organic Aerosols, Life, 11, 319, 2021.
Ling, Z., Wu, L., Wang, Y., Shao, M., Wang, X., and Huang, W.: Roles of semivolatile and intermediate-volatility organic compounds in secondary organic aerosol formation and its implication: A review, J. Environ. Sci. (China), 114, 259-285, 10.1016/j.jes.2021.08.055, 2022.
Liu, T., Wang, X., Deng, W., Hu, Q., Ding, X., Zhang, Y., He, Q., Zhang, Z., Lü, S., Bi, X., Chen, J., and Yu, J.: Secondary organic aerosol formation from photochemical aging of light-duty gasoline vehicle exhausts in a smog chamber, Atmos. Chem. Phys., 15, 9049-9062, 10.5194/acp-

15-9049-2015, 2015.
Majdi, M., Sartelet, K., Lanzafame, G. M., Couvidat, F., Kim, Y., Chrit, M., and Turquety, S.: Precursors and formation of secondary organic aerosols from wildfires in the Euro-Mediterranean region, Atmos. Chem. Phys., 19, 5543-5569, 10.5194/acp-19-5543-2019, 2019.
Pye, H. O. and Pouliot, G. A.: Modeling the role of alkanes, polycyclic aromatic hydrocarbons, and their oligomers in secondary organic aerosol formation, Environ. Sci. Technol., 46, 6041-6047, 10.1021/es300409w, 2012.
Pye, H. O. T. and Seinfeld, J. H.: A global perspective on aerosol from low-volatility organic compounds, Atmos. Chem. Phys., 10, 4377-4401, 10.5194/acp-10-4377-2010, 2010.
Qin, M., Hu, A., Mao, J., Li, X., Sheng, L., Sun, J., Li, J., Wang, X., Zhang, Y., and Hu, J.: PM2.5 and O3 relationships affected by the atmospheric oxidizing capacity in the Yangtze River Delta, China, Sci. Total Environ., 810, 152268, https://doi.org/10.1016/j.scitotenv.2021.152268, 2022.
Riva, M., Healy, R. M., Flaud, P.-M., Perraudin, E., Wenger, J. C., and Villenave, E.: Kinetics of the Gas-Phase Reactions of Chlorine Atoms with Naphthalene, Acenaphthene, and Acenaphthylene, J. Phys. Chem. A, 118, 3535-3540, 10.1021/jp5009434, 2014.
Riva, M., Healy, R. M., Flaud, P.-M., Perraudin, E., Wenger, J. C., and Villenave, E.: Gas- and Particle-Phase Products from the Chlorine-Initiated Oxidation of Polycyclic Aromatic Hydrocarbons, J. Phys. Chem. A, 119, 11170-11181, 10.1021/acs.jpca.5b04610, 2015.
Robinson, A. L., Donahue, N. M., Shrivastava, M. K., Weitkamp, E. A., Sage, A. M., Grieshop, A. P., Lane, T. E., Pierce, J. R., and Pandis, S. N.: Rethinking organic aerosols: semivolatile emissions and photochemical aging, Science, 315, 1259-1262, 10.1126/science.1133061, 2007.
Shakya, K. M. and Griffin, R. J.: Secondary Organic Aerosol from Photooxidation of Polycyclic Aromatic Hydrocarbons, Environ. Sci. Technol., 44, 8134-8139, 10.1021/es1019417, 2010.
Tan, Z., Lu, K., Hofzumahaus, A., Fuchs, H., Bohn, B., Holland, F., Liu, Y., Rohrer, F., Shao, M., Sun, K., Wu, Y., Zeng, L., Zhang, Y., Zou, Q., Kiendler-Scharr, A., Wahner, A., and Zhang, Y.: Experimental budgets of OH, HO2, and RO2 radicals and implications for ozone formation in the Pearl River Delta in China 2014, Atmos. Chem. Phys., 19, 7129-7150, 10.5194/acp-19-7129-2019, 2019.
Tang, T., Cheng, Z., Xu, B., Zhang, B., Zhu, S., Cheng, H., Li, J., Chen, Y., and Zhang, G.: Triple Isotopes (δ13C, δ2H, and Δ14C) Compositions and Source Apportionment of Atmospheric Naphthalene: A Key Surrogate of Intermediate-Volatility Organic Compounds (IVOCs), Environ. Sci. Technol., 54, 5409-5418, 10.1021/acs.est.0c00075, 2020.
Tham, Y. J., Yan, C., Xue, L., Zha, Q., Wang, X., and Wang, T.: Presence of high nitryl chloride in Asian coastal environment and its impact on atmospheric photochemistry, Chin. Sci. Bull., 59, 356-359, 10.1007/s11434-013-0063-y, 2014.
Tuet, W. Y., Chen, Y., Fok, S., Gao, D., Weber, R. J., Champion, J. A., and Ng, N. L.: Chemical and cellular oxidant production induced by naphthalene secondary organic aerosol (SOA): effect of redox-active metals and photochemical aging, Sci. Rep., 7, 15157, 10.1038/s41598-017-15071-8, 2017a.
Tuet, W. Y., Chen, Y., Xu, L., Fok, S., Gao, D., Weber, R. J., and Ng, N. L.: Chemical oxidative potential of secondary organic aerosol (SOA) generated from the photooxidation of biogenic and anthropogenic volatile organic compounds, Atmos. Chem. Phys., 17, 839-853, 10.5194/acp-17-839-2017, 2017b.
Wang, H., Chen, X., Lu, K., Hu, R., Li, Z., Wang, H., Ma, X., Yang, X., Chen, S., Dong, H., Liu, Y., Fang, X., Zeng, L., Hu, M., and Zhang, Y.: NO3 and N2O5 chemistry at a suburban site during the EXPLORE-YRD campaign in 2018, Atmos. Environ., 224, 10.1016/j.atmosenv.2019.117180,

2020a.
Wang, L., Arey, J., and Atkinson, R.: Reactions of Chlorine Atoms with a Series of Aromatic Hydrocarbons, Environ. Sci. Technol., 39, 5302-5310, 10.1021/es0479437, 2005.
Wang, M., Chen, D., Xiao, M., Ye, Q., Stolzenburg, D., Hofbauer, V., Ye, P., Vogel, A. L., Mauldin, R. L., Amorim, A., Baccarini, A., Baumgartner, B., Brilke, S., Dada, L., Dias, A., Duplissy, J., Finkenzeller, H., Garmash, O., He, X.-C., Hoyle, C. R., Kim, C., Kvashnin, A., Lehtipalo, K., Fischer, L., Molteni, U., Petäjä, T., Pospisilova, V., Quéléver, L. L. J., Rissanen, M., Simon, M., Tauber, C., Tomé, A., Wagner, A. C., Weitz, L., Volkamer, R., Winkler, P. M., Kirkby, J., Worsnop, D. R., Kulmala, M., Baltensperger, U., Dommen, J., El-Haddad, I., and Donahue, N. M.: Photo-oxidation of Aromatic Hydrocarbons Produces Low-Volatility Organic Compounds, Environ. Sci. Technol., 54, 7911-7921, 10.1021/acs.est.0c02100, 2020b.
Wang, S., Ye, J., Soong, R., Wu, B., Yu, L., Simpson, A. J., and Chan, A. W. H.: Relationship between chemical composition and oxidative potential of secondary organic aerosol from polycyclic aromatic hydrocarbons, Atmos. Chem. Phys., 18, 3987-4003, 10.5194/acp-18-3987-2018, 2018.
Wang, X., Li, L., Gong, K., Mao, J., Hu, J., Li, J., Liu, Z., Liao, H., Qiu, W., Yu, Y., Dong, H., Guo, S., Hu, M., Zeng, L., and Zhang, Y.: Modelling air quality during the EXPLORE-YRD campaign – Part I. Model performance evaluation and impacts of meteorological inputs and grid resolutions, Atmos. Environ., 246, 10.1016/j.atmosenv.2020.118131, 2021.
Wiedinmyer, C., Akagi, S. K., Yokelson, R. J., Emmons, L. K., Al-Saadi, J. A., Orlando, J. J., and Soja, A. J.: The Fire INventory from NCAR (FINN): a high resolution global model to estimate the emissions from open burning, Geosci. Model Dev., 4, 625-641, 10.5194/gmd-4-625-2011, 2011.
Yu, Y., Wang, H., Wang, T., Song, K., Tan, T., Wan, Z., Gao, Y., Dong, H., Chen, S., Zeng, L., Hu, M., Wang, H., Lou, S., Zhu, W., and Guo, S.: Elucidating the importance of semi-volatile organic compounds to secondary organic aerosol formation at a regional site during the EXPLORE-YRD campaign, Atmos. Environ., 246, 10.1016/j.atmosenv.2020.118043, 2021.
Zhang, H. and Ying, Q.: Secondary organic aerosol formation and source apportionment in Southeast Texas, Atmos. Environ., 45, 3217-3227, 10.1016/j.atmosenv.2011.03.046, 2011.
Zhang, H. and Ying, Q.: Secondary organic aerosol from polycyclic aromatic hydrocarbons in Southeast Texas, Atmos. Environ., 55, 279-287, 2012.
Zhang, J., Wang, P., Li, J., Mendola, P., Sherman, S., and Ying, Q.: Estimating population exposure to ambient polycyclic aromatic hydrocarbon in the United States - Part II: Source apportionment and cancer risk assessment, Environ. Int., 97, 163-170, 10.1016/j.envint.2016.08.024, 2016.
Zhang, Y. and Tao, S.: Global atmospheric emission inventory of polycyclic aromatic hydrocarbons (PAHs) for 2004, Atmos. Environ., 43, 812-819, 10.1016/j.atmosenv.2008.10.050, 2009.
Zhu, J., Wang, S., Wang, H., Jing, S., Lou, S., Saiz-Lopez, A., and Zhou, B.: Observationally constrained modeling of atmospheric oxidation capacity and photochemical reactivity in Shanghai, China, Atmos. Chem. Phys., 20, 1217-1232, 10.5194/acp-20-1217-2020, 2020.

612 **Table 1.** Settings of the scenarios.

Case	Emission setting	SOA parameterization for MN
case-1product-orig	Nap emissions in the YRD were based on the 2017 YRD inventory; Nap emissions in the rest of the domain and MN emissions in the entire domain were calculated using sector-specific mass ratios and total emissions of non-methane volatile organic compounds (emis-orig)	one-product method
case-2products-orig		two-product method
case-1product	The anthropogenic emissions of Nap and MN in the entire domain from emis-orig were multiplied by 5 and 7, respectively (emis-adjust)	one-product method
case-2products		two-product method
base_zeroNapMN	Emissions of Nap and MN were set to zero based on emis-adjust	one-product method
base_zeroMN	Emissions of MN were set to zero based on emis-adjust	one-product method

613

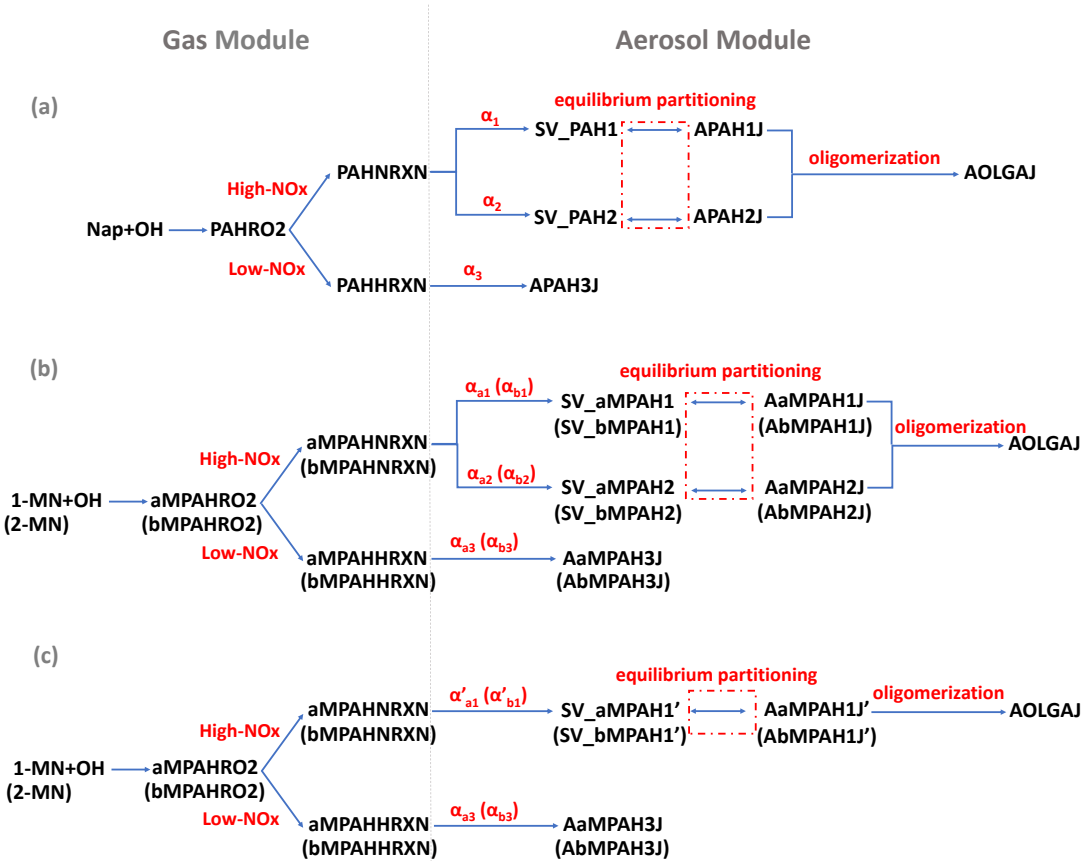

614

615 **Figure 1.** SOA schemes for naphthalene (Nap), 1-methylnaphthalene (1-MN), and 2-
616 methylnaphthalene (2-MN) in the updated CMAQ model. (a) pre-existing Nap-derived SOA
617 formation pathways fitted by two products under high NO_x; (b) newly added SOA formation
618 pathways for 1-MN and 2-MN fitted by two products under high NO_x; (c) newly added SOA
619 formation pathways for 1-MN and 2-MN fitted by one product under high NO_x. SOA formation
620 from Nap and MN oxidation by OH radicals under low-NO_x conditions is represented by a fixed
621 yield. Parameters for 2-MN are indicated in brackets in (b) and (c). The values of α refer to Table
622 S1.

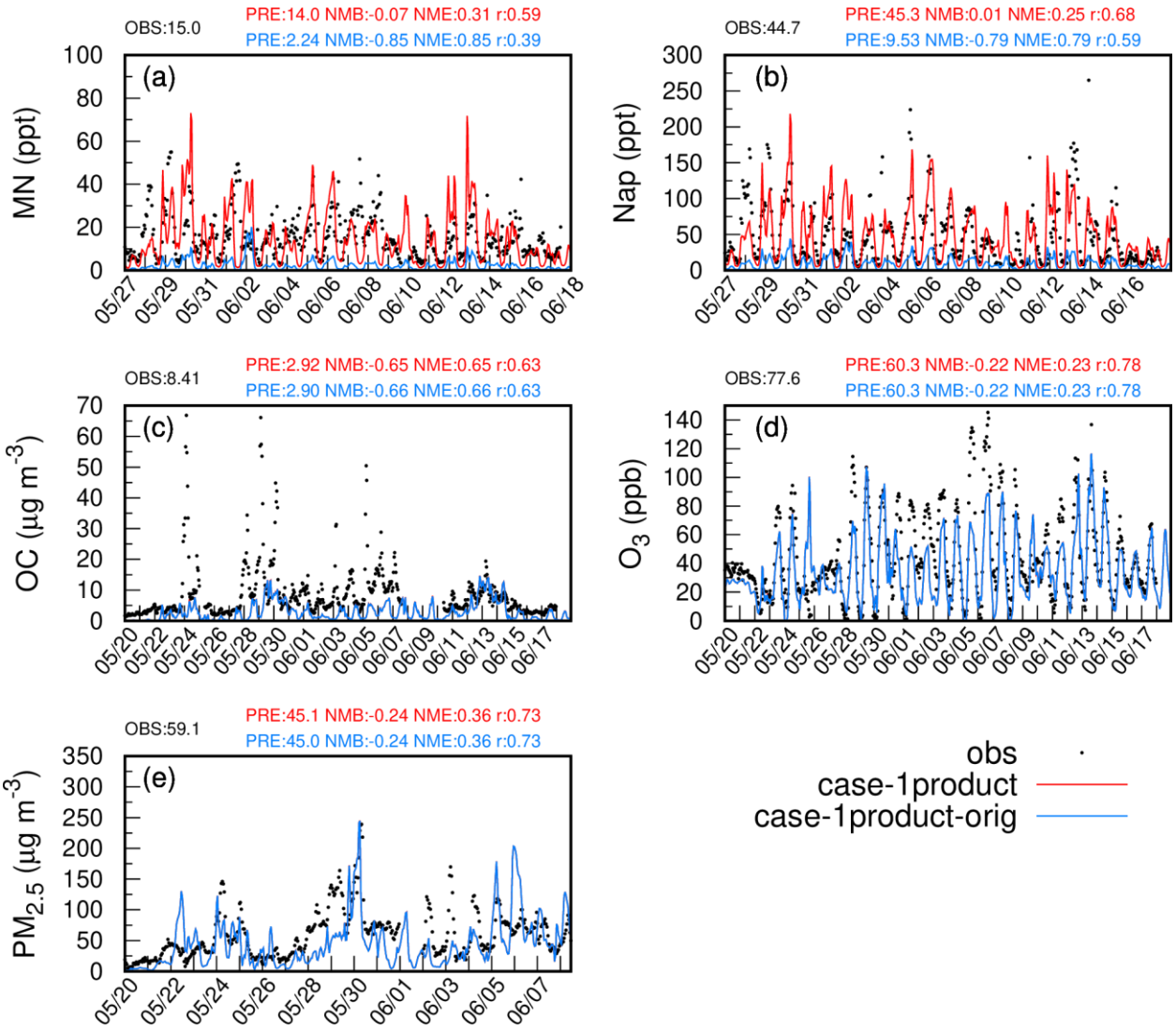

623

624 **Figure 2.** Observed and simulated hourly concentrations of MN, Nap, OC, $PM_{2.5}$, and O_3 based
625 on emis-adjust (red) and emis-orig (blue) at the Taizhou site. Model performances for daily MN,
626 Nap, OC, $PM_{2.5}$, and MDA8 O_3 are shown in blue for case-1product-orig and in red for case-
627 1product. OBS and PRE represent the average of observations and predictions, respectively. Note
628 that the red and blue lines overlap in (c)-(e).

629

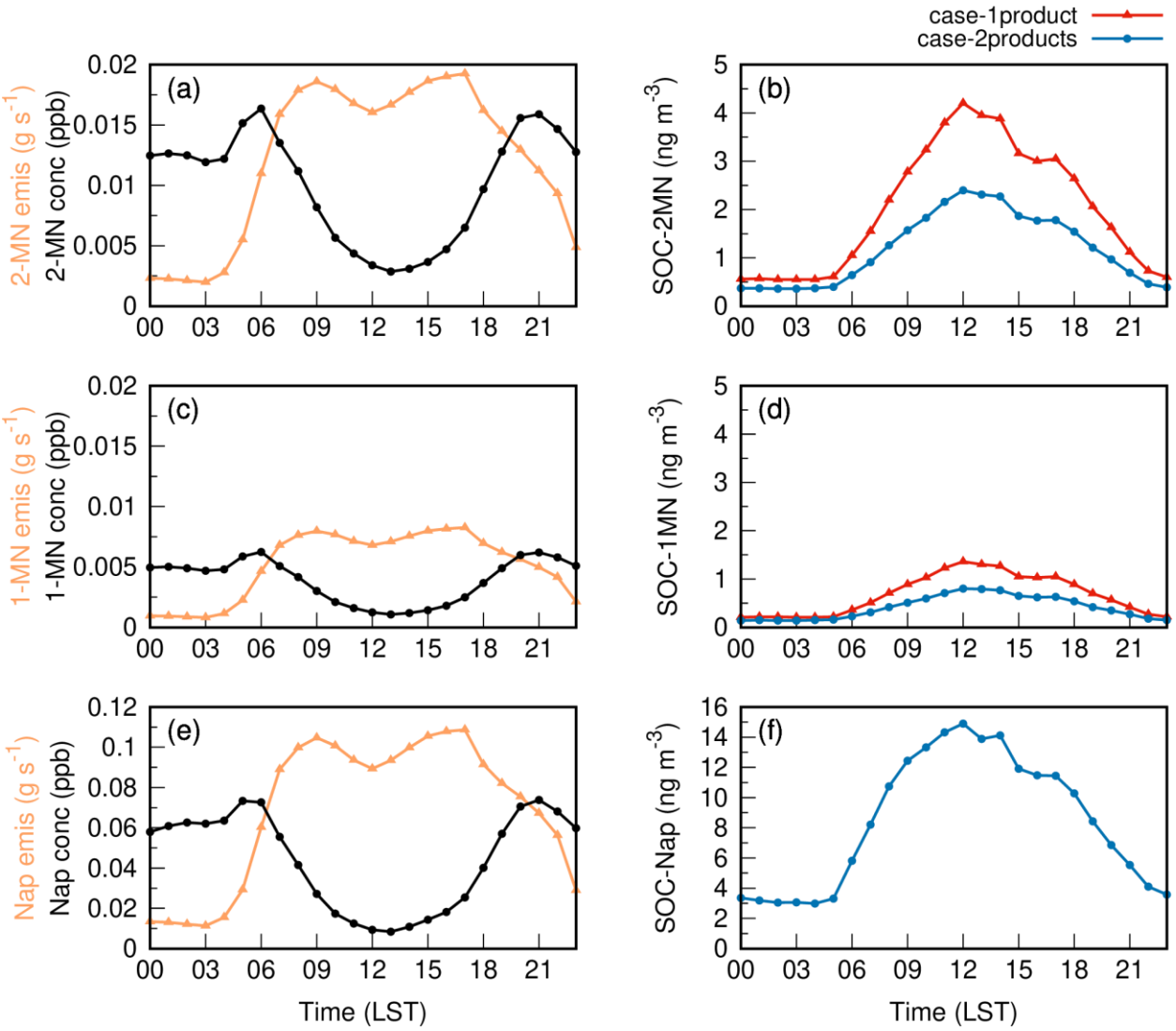

630

631 **Figure 3.** Diurnal variations of emissions (yellow line) and predicted concentrations (black line)

632 for 2-MN (a), 1-MN (c), and Nap (e), as well as the corresponding SOC concentrations (b, d, f) at

633 the Taizhou site. Note that the red and blue lines overlap in (f).

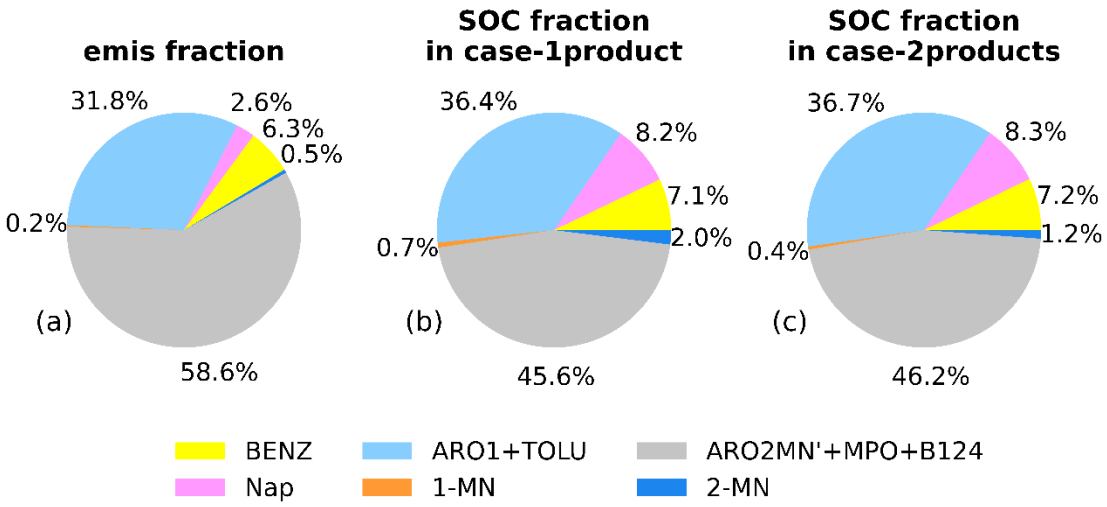

634

635 **Figure 4.** Contributions of the major aromatic species to (a) the total emissions of aromatics
636 (weight fraction) and the aromatic-derived SOC in (b) case-1product and (c) case-2products at the
637 Taizhou site. The aromatic species include Nap, 1-MN, 2-MN, BENZ, the sum of toluene and
638 aromatics with $k_{OH} < 2x10^4$ ppm^{-1} min^{-1} (ARO1+TOLU), and the sum of xylenes, 1,2,4-trimethyl
639 benzene and aromatics with $k_{OH} > 2x10^4$ ppm^{-1} min^{-1} excluding Nap and MN
640 (ARO2MN'+MPO+B124).

641

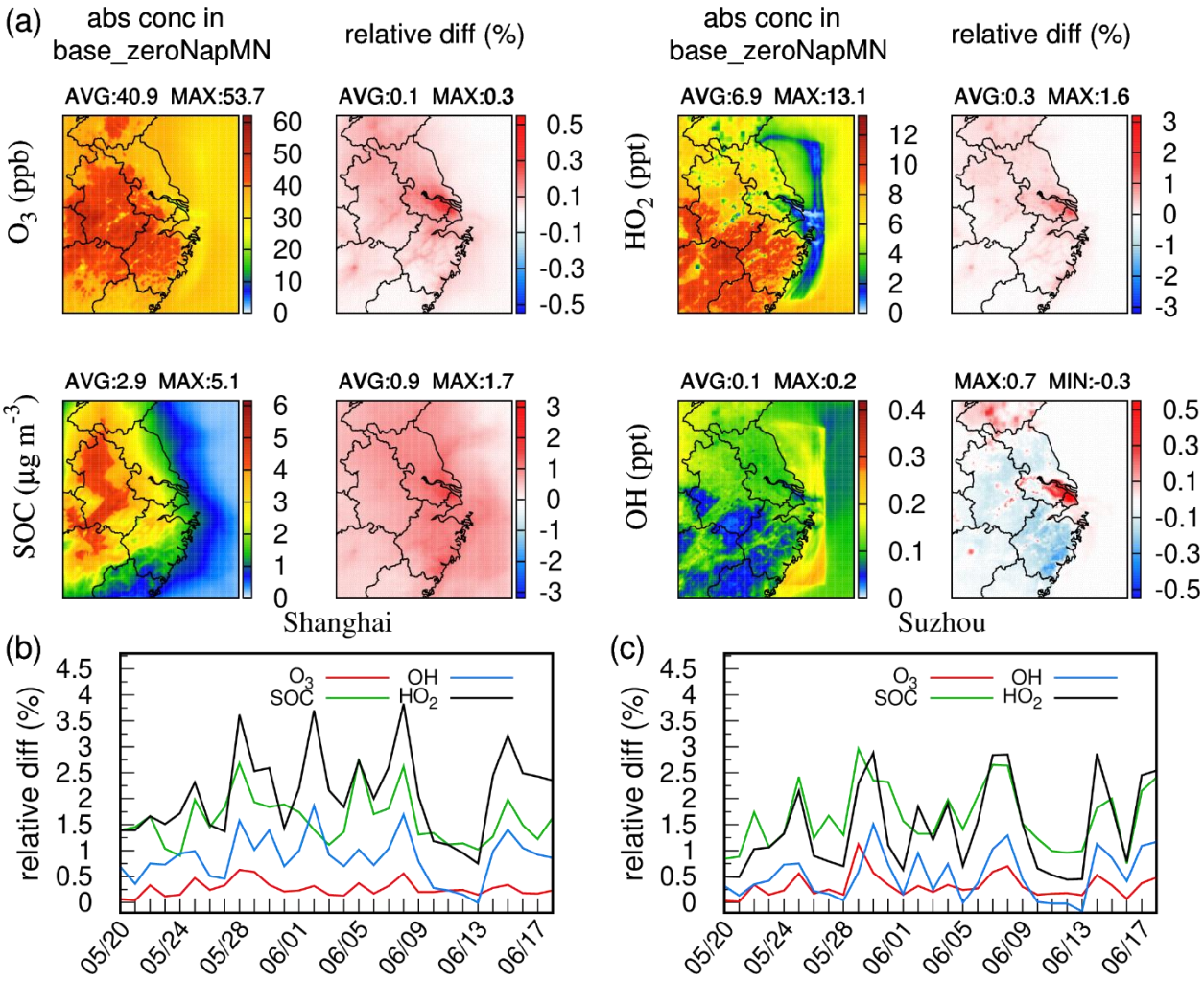

Figure 5. (a) Average concentrations of SOC, O_3, OH·, and HO_2· in base_zeroNapMN and changes in case-1product relative to base_zeroNapMN. Daily relative changes in case-1product compared to base_zeroNapMN in (b) Shanghai and (c) Suzhou.